Research Square

Preprints are preliminary reports that have not undergone peer review.
They should not be considered conclusive, used to inform clinical practice,
or referenced by the media as validated information.

Can pure-gas permeability data design a mixed-gas module? A correctability map for dual-mode CO2/N2 transport in Matrimid 5218 hollow fibres

Miracle Ajoku

miracleajoku96@gmail.com

Federal University of Technology Owerri https://orcid.org/0009-0001-2256-3651

Modade Sola-Ojo

Landmark University https://orcid.org/0009-0000-4682-4759

George Chukwuebuka Duru

Federal University of Technology Owerri https://orcid.org/0009-0003-0542-737X

Research Article

Keywords: Dual-mode sorption, Matrimid 5218, Hollow-fibre module, CO2/N2 separation, Mixed-gas permeation, Membrane module design

Posted Date: November 9th, 2026

DOI: https://doi.org/10.21203/rs.3.rs-11646086/v1

License: This work is licensed under a Creative Commons Attribution 4.0 International License.
Read Full License

Additional Declarations: The authors declare no competing interests.

Can pure-gas permeability data design a mixed-gas module? A correctability map for dual-mode CO_2/N_2 transport in Matrimid 5218 hollow fibres

Miracle Victory Ajoku[1*], Modade Sola-Ojo [2], George Chukwuebuka Duru[1]

[1]Department of Chemical Engineering, Federal University of Technology Owerri, Owerri, Imo State, Nigeria

[2] Department of Chemical Engineering, Landmark University, Omu-Aran, Kwara State, Nigeria

*Corresponding author E-mail: miracleajoku96@gmail.com

Abstract

Pure-gas permeabilities are routinely used to size polymeric gas-separation modules, although permeation in glassy polymers depends on pressure and composition through dual-mode sorption. This work asks whether any choice of pure-gas measurement pressure can make such data reproduce mixed-gas module performance, using CO_2/N_2 in Matrimid 5218 as a case study. An exact partial-immobilization flux with competitive sorption on both membrane faces was embedded in a mass-balance-verified counter-current hollow-fibre model. The governing mobility parameter F·K was calibrated against two independent literature datasets (0.191; 90% confidence interval 0.123–0.272), whereas a single-laboratory literature value (0.859) failed a held-out test. With pure-gas data taken at 1 bar, the design overestimated CO_2 recovery by 2.5 to 3.5 percentage points (1.7–4.8 across the F·K interval) and CO_2 purity by 0.7–1.2 points, corresponding to modules undersized by 5.6–9.6% of the area actually required. Whether this bias can be removed by choosing another measurement pressure depends jointly on feed CO_2 partial pressure and stage cut. At stage cuts of about 10–13%, no measurement pressure corrects the design below a feed CO_2 partial pressure of about 0.84 bar, and correction within 20 bar requires more than about 1.64 bar; this uncorrectable regime contracts with increasing

stage cut and was not observed above roughly 18%. It arises where competitive sorption depresses the local mixed-gas CO_2 permeability below the pure-gas Henry's-law limit. Higher temperature reduces the bias but costs more in selectivity. The results identify where mixed-gas characterization cannot be replaced by pure-gas testing. Mapped onto industrial CO_2 sources at 10 bar feed, natural-gas combined-cycle flue gas falls in the uncorrectable regime, coal flue gas in a regime correctable only by impractically high test pressures, and enriched or cement-kiln feeds in a regime correctable by routine testing. A screening procedure is proposed that tells the designer, before any module is sized, whether vendor pure-gas data are adequate, require a stated area margin, or must be replaced by mixed-gas measurements.

Keywords: Dual-mode sorption; Matrimid 5218; Hollow-fibre module; CO_2/N_2 separation; Mixed-gas permeation; Membrane module design

1. Introduction

Polymeric membranes are an established option for CO_2/N_2 separation in post-combustion capture, biogas upgrading and inert-gas generation, owing to their compactness, absence of chemical solvents and modular scale-up (Baker and Lokhandwala 2008; Merkel et al. 2010). Module design for these applications almost always starts from permeabilities measured with single gases, which are then treated as constants in a module or process model. For rubbery polymers and many dilute systems this is an acceptable simplification. For glassy polymers, which dominate commercial gas-separation membranes, it is not guaranteed to be.

Sorption and transport in glassy polymers below the glass transition are commonly described by the dual-mode model, in which penetrant molecules partition between a Henry's-law population dissolved in the densified matrix and a Langmuir population held in non-equilibrium excess free volume (Paul and Koros 1976). Although alternative frameworks exist, the dual-mode model remains the reference description for glassy membrane transport (Minelli

and Sarti 2020). Because the Langmuir population saturates with pressure and is shared competitively between co-sorbing species, the permeability of a glassy polymer depends on the partial pressure of the permeating gas and on the composition of the mixture. Mixed-gas CO_2 permeabilities in glassy polyimides are therefore frequently lower than pure-gas values at the same partial pressure (Heck et al. 2017).

The consequences for module design have been examined in several ways. Module models that allow permeance to vary with local pressure, temperature or composition have been shown to predict different separation performance, required membrane area and process economics than constant-permeance models (Khalilpour et al. 2013; Ahmad et al. 2013; Bounaceur et al. 2017). In parallel, sorption studies have shown that dual-mode parameter sets which describe pure-gas isotherms equally well can diverge substantially in their mixed-gas predictions (Ricci and De Angelis 2019), and that parameter uncertainty propagates strongly into mixture predictions (Monsalve-Bravo et al. 2024). Inter-laboratory comparisons show that even pure-gas permeabilities of a commercial polymer can differ appreciably between laboratories (Mizrahi Rodriguez et al. 2022). The transport parameters that would be needed to correct a pure-gas design are therefore themselves uncertain.

These studies quantify the error that follows from a particular constant-permeability assumption. They do not address a question that the experimentalist can act on directly: whether the choice of pure-gas measurement pressure can be used to remove the error, and under which feed and operating conditions it cannot. If a measurement pressure exists at which pure-gas data happen to reproduce the true mixed-gas module performance, that pressure is a practical target for screening protocols. If no such pressure exists, mixed-gas characterization cannot be replaced by more careful pure-gas testing. To the authors' knowledge, no criterion separating these cases has been reported, nor has it been examined whether the answer depends on how the module is operated.

The question has direct engineering consequences. Membrane vendors and process engineers routinely size modules from pure-gas permeances supplied on data sheets, because mixed-gas permeation at process-relevant pressures and compositions is slower, more expensive and rarely available at the screening stage. In post-combustion capture the membrane is the largest single capital item of the separation unit, and its area is set to meet a recovery and purity specification for downstream compression and storage (Merkel et al. 2010). An optimistic permeance therefore propagates into a module that misses its capture target, into recompression and vacuum equipment sized for the wrong permeate flow, and into cost estimates that omit part of the membrane area. Knowing in advance which feeds can be designed safely from pure-gas data, and which cannot, would allow mixed-gas testing to be targeted at the cases where it changes the design.

This work addresses that question for CO_2/N_2 in Matrimid 5218, a widely studied glassy polyimide for which dual-mode sorption and diffusion parameters are available (Moore and Koros 2007; David et al. 2011a; Scholes et al. 2010). An exact two-face dual-mode flux, with competitive sorption and finite downstream pressure on both membrane faces, is embedded in a counter-current hollow-fibre model and used to (i) calibrate the dual-mode mobility parameter against independent literature data and test its transferability between laboratories; (ii) quantify the recovery, purity and membrane-area error of a pure-gas design; (iii) define a correctability boundary and map it over feed CO_2 partial pressure and stage cut; (iv) decompose the design error into CO_2 self-suppression and N_2 competition; and (v) assess how temperature changes the error. The study is a modelling analysis: it isolates the dual-mode contribution and does not include fibre-bore pressure drop, plasticization or non-isothermal effects, which are discussed as limitations in Section 4.10. Section 4.9 translates the results into design terms for representative industrial CO_2 sources.

2. Methods: theoretical framework

2.1. Dual-mode sorption with competitive Langmuir equilibrium

The equilibrium concentration of penetrant *i* in the polymer is the sum of a Henry's-law and a Langmuir contribution (Paul and Koros 1976):

$$C_i = k_{D,i}\, p_i + \frac{C'_{H,i} b_i p_i}{1 + b_i p_i + \sum_{j \neq i} b_j p_j} \quad (1)$$

where $k_{D,i}$ is the Henry's-law coefficient, $C'_{H,i}$ the Langmuir capacity, b_i the Langmuir affinity constant and the sum accounts for competitive displacement by co-sorbed species *j*. In the partial-immobilization model the Langmuir population diffuses with coefficient D_H, distinct from the Henry's-law diffusion coefficient D_D. With $F = D_H/D_D$ and $K = C'_H b/k_D$, the product $F \cdot K$ sets the magnitude of pressure-dependent permeability in this model and is the principal parameter calibrated in Section 3.2.

2.2. Exact two-face flux and the Henry's-law floor

For steady one-dimensional transport across a dense layer of thickness *l*, with local equilibrium between the two populations at each face and constant D_D and D_H, integration of Fick's law for each population gives (Paul and Koros 1976):

$$N_i \cdot l = D_{D,i}\left(C_{D,i,feed} - C_{D,i,perm}\right) + D_{H,i}\left(C_{H,i,feed} - C_{H,i,perm}\right) \quad (2)$$

where both concentrations at each face are evaluated from Eq. (1) using the local partial pressures of *i* and of the co-permeant on that face. Eq. (2) therefore retains competitive sorption and non-zero downstream pressure on both faces. When the permeate-side partial pressures are set to zero and no co-permeant is present, Eq. (2) reduces to the closed-form pure-gas permeability of Paul and Koros (1976):

$$P_i(p) = k_{D,i}\, D_{D,i}\left(\frac{1 + F_i K_i}{1 + b_i p_i}\right) \quad (3)$$

Eq. (3) decreases monotonically with pressure towards the Henry's-law floor $P_\infty = k_D D_D$, which is the lowest value any pure-gas measurement can return. The implemented Eq. (2) reproduced Eq. (3) to within 10^{-14} (relative) in the vacuum-downstream limit at all pressures tested. In a mixture, Eq. (2) is not bounded by P_∞: where competition depresses C_H on the feed face more strongly than on the permeate face, the Langmuir term can vanish or change sign, and the local mixed-gas permeability can fall below the pure-gas floor. This property underlies the uncorrectable regime identified in Section 4.4.

2.3. Counter-current hollow-fibre module

The module is a bundle of parallel fibres in counter-current flow with feed on the shell side and permeate in the bore, following standard permeator formulations (Thundyil and Koros 1997). The component balances are

$$\frac{dF_{c,feed}}{dz} = -aJ_c(Z);\ \frac{dF_{n,feed}}{dz} = -aJ_n(z) \quad (4)$$

$$\frac{dF_{c,perm}}{dz} = -aJ_c(Z);\ \frac{dF_{n,perm}}{dz} = -aJ_n(z) \quad (5)$$

with $F_{c,feed}(0) = F_{c,in}$, $F_{n,feed}(0) = F_{n,in}$ at the feed inlet and $F_{c,perm}(L) = F_{n,perm}(L) = 0$ at the closed end of the permeate channel, where subscripts c and n denote CO_2 and N_2 and a is the membrane area per unit length. The local fluxes J follow from Eq. (2) with the local feed- and permeate-side compositions. The reference module has 10,000 fibres of 300 μm outer diameter and 1.0 m active length (A = 9.42 m^2). Feed pressure is 5–20 bar, permeate pressure 1 bar, and pressure drop on both sides is neglected.

The feed flow rate is set relative to the flux that a pure-gas design predicts at the inlet:

$$F_{in} = \varphi A\left[P_{ref,CO2}\, y + P_{ref\cdot N2}\,(1-y)\right]\frac{P_{feed}-P_{perm}}{l} \quad (6)$$

with $P_{ref,CO2}$ = 5.5 Barrer, $P_{ref,N2}$ = 0.19 Barrer and φ = 5 in the baseline, which yields Model B stage cuts of about 10–13% at 10 bar. Because stage cut proved to be a controlling variable, φ was varied from 2 to 15 (stage cuts of about 4–44%) in Sections 4.3 and 4.4. A dense-layer thickness l = 50 μm was used. Since the model depends on thickness only through the group (permeance × area / feed flow), all reported quantities are independent of l when F_{in} is scaled accordingly; this was confirmed numerically for l = 50, 5 and 0.5 μm, which gave identical recoveries and biases to all reported digits (Supplementary file 1: Table S1).

2.4. Pure-gas design, true mixed-gas performance and design error

Two descriptions of the same module are compared at identical feed conditions. In Model A (pure-gas design), the CO_2 permeability is Eq. (3) evaluated at a single measurement pressure p_{ref} and applied uniformly along the module; N_2 permeability is 0.19 Barrer. In Model B (true mixed-gas performance), Eq. (2) is evaluated locally at every axial position. The recovery and purity biases are

$$\Delta Rec(p_{ref}) = Rec_A(p_{ref}) - Rec_B;\ \Delta\mathrm{Pur}(\mathrm{p_{ref}}) = \mathrm{Pur_A}(\mathrm{p_{ref}}) - \mathrm{Pur_B} \quad (7)$$

A positive bias means that the pure-gas design is optimistic. To express the error in design terms, the area A_A that Model A requires to reach a target CO_2 recovery was compared with the area A_B that Model B requires for the same feed. Because recovery depends on area only through the ratio A/F_{in}, this was evaluated by solving for the feed flow that gives the target recovery in the fixed reference module, so that $A_B/A_A = F_{in,A}/F_{in,B}$. The area error is

$$\varepsilon_A = 1 - \frac{A_A}{A_B} \quad (8)$$

which is the fraction of the truly required area that the pure-gas design omits.

2.5. Correctability boundary

The correcting measurement pressure p^* is defined by $\Delta\mathrm{Rec}(p^*) = 0$: the pure-gas test pressure at which Model A reproduces the true recovery. Its existence can be tested exactly. Eq. (3) is strictly decreasing in p_{ref} for $F{\cdot}K > 0$ and tends to P_∞. For fixed N_2 permeability, feed and geometry, the recovery of a counter-current separator with spatially uniform permeability is strictly increasing in the CO_2 permeability, since a higher permeability raises the local CO_2 flux at every position without changing the N_2 flux. $\mathrm{Rec_A}(p_{\mathrm{ref}})$ is therefore strictly decreasing and continuous, and so is ΔRec. A root exists if and only if the limiting value $\Delta\mathrm{Rec}_\infty = \mathrm{Rec_A}(P_\infty) - \mathrm{Rec_B}$ is negative. Three regimes follow: *structural* ($\Delta\mathrm{Rec}_\infty > 0$, no measurement pressure corrects the design); *correctable but impractical* (p^* exists but exceeds 20 bar); and *practical* ($p^* \leq 20$ bar). The 20 bar limit is a representative upper bound for routine pure-gas characterization rather than a physical constant; p^* values are reported so that other limits can be applied.

2.6. Numerical solution

Eqs. (4) to (5) were discretized into N axial cells and solved by Gauss–Seidel iteration with alternating-direction sweeps of the feed and permeate channels and a fixed relaxation factor $\omega = 0.4$. Convergence was accepted only when the CO_2 mass-balance error, $|F_{\mathrm{c,in}} - F_{\mathrm{c,perm,out}} - F_{\mathrm{c,ret}}|/F_{\mathrm{c,in}}$, fell below 0.005%; if not, the iteration budget and the iterate-change tolerance were tightened together and the solution repeated. Reducing ω between retries was avoided because, with a fixed iterate-change tolerance, it can signal convergence before the state has converged. Roots in p_{ref}, feed composition and feed flow were located with Brent's method, p^* in $\log(p_{\mathrm{ref}})$ over 0.25 bar to 10^6 bar, the latter representing P_∞.

A grid study at the reference condition (35 °C, 15% CO_2, 10 bar) over N = 25–200 showed first-order convergence (Online Resource 1, Fig. S1b). Successive changes in ΔRec(1 bar) on doubling N were +0.028, +0.014 and +0.007 percentage points (pp), giving an extrapolated

value of 2.561 pp against 2.532 pp at $N = 50$. The production resolution $N = 50$ therefore carries an error of about 0.03 pp (1.1%) on the bias, ten times smaller than its error on absolute recovery (about 0.27 pp), because discretization errors largely cancel between Models A and B. Mass-balance errors of all reported solutions were below 0.005%. All calculations were performed in Python with NumPy and SciPy. Generative AI (Claude, Anthropic) was used under the authors' direction to assist with writing the analysis code and the structural flow and refinement of the manuscript text; the authors designed the study, verified all code, results and text, and take full responsibility for the content.

3. Methods: parameters and calibration

3.1. Sorption and diffusion parameters

Table 1 lists the parameters at 35 °C. CO_2 and N_2 sorption parameters are from Moore and Koros (2007). CO_2 diffusion coefficients are those fitted by David et al. (2011a), which give P = 5.464 Barrer at 4 bar; when $F \cdot K$ is changed, D_D is re-solved so that Eq. (3) keeps this value at 4 bar, so that the calibration changes the pressure dependence of the permeability but not its level at the anchor pressure. N_2 is assumed fully immobilized in the Langmuir population (F_{N2} = 0), for which no independent measurement exists, and $D_{D,N2}$ is set to give 0.19 Barrer, consistent with the value reported for Matrimid at 2 bar and 30 °C by David et al. (2011b). The consequences of $F_{N2} = 0$ are quantified in Section 4.7.

Table 1 Dual-mode parameters for Matrimid 5218 at 35 °C

Parameter	Units	CO_2	N_2	Source
k_D	$cm^3(STP)\ cm^{-3}\ bar^{-1}$	1.42	0.118	(Moore and Koros 2007)
C'_H	$cm^3(STP)\ cm^{-3}$	25.5	3.94	(Moore and Koros 2007)
b	bar^{-1}	0.367	0.087	(Moore and Koros 2007)
$K = C'_H b/k_D$	–	6.59	2.89	Calculated

Parameter	Units	CO_2	N_2	Source
$F \cdot K$, calibrated (primary)	–	0.191 (0.123–0.272)	0	Section 3.2
$F = D_H/D_D$, calibrated	–	0.029	0[a]	Section 3.2
$F \cdot K$, single-laboratory fit	–	0.859	–	(David et al. 2011a)[b]
P(4 bar), pure gas	Barrer	5.464	0.19[c]	(David et al. 2011a, b)
$P_\infty = k_D D_D$ (at $F \cdot K = 0.191$)	Barrer	5.071	0.19	Eq. (3)

[a] Assumed; sensitivity in Section 4.7. [b] Derived from $D_H/D_D = 0.1303$ fitted by David et al.; retained only as a comparison. [c] Pressure-independent under $F_{N2} = 0$.

3.2. Calibration of F·K against independent data

The single-laboratory value $F \cdot K = 0.859$ (David et al. 2011a) was obtained by fitting the same group's H_2/CO_2 permeation data, so it cannot be validated against those data. $F \cdot K$ was therefore calibrated against two datasets from other laboratories, each expressed in a form that does not require the absolute permeability to agree.

Bos et al. (1999) report, for Matrimid, a pure-CO_2 permeability of 5.7 Barrer extrapolated to zero pressure and a minimum of 4.8 Barrer at the plasticization pressure of 12 bar. Only these two values are used. With $R = P(12)/P(0)$, Eq. (3) gives $F \cdot K = (R - 1)/[1/(1 + 12b) - R] = 0.240$. Uncertainty was propagated by Monte Carlo sampling (5000 draws) with a 3% relative standard uncertainty on each permeability, typical of single-gas permeation, and with 5% as a sensitivity case. An earlier version of this analysis that fitted eight points interpolated from a curve through these two values was discarded, because resampling interpolated points understates the uncertainty.

Esposito et al. (2019) report the CO_2 permeability of Matrimid in a 15/85 CO_2/N_2 mixture at twelve total pressures between 1 and 6 bar at 25 °C. The model shape, Eq. (3) with competitive N_2 in the denominator, was fitted with a free amplitude, so that only the pressure dependence is used, and the residuals were expressed as fractions of that amplitude. Uncertainty was obtained by bootstrap resampling of the twelve points (5000 resamples, independent seed). The fitted value was converted from 25 to 35 °C through the temperature dependence of K (Section 3.3), a factor of 0.948, with F held constant.

The two estimates were combined with inverse-variance weights. The results are summarized in Table 2 and discussed in Section 4.2. The combined median, 0.192, is used as the primary value (0.191 in all computations; the difference is negligible), with the 90% interval 0.123–0.272 propagated through all principal results. The implied mobility ratio is $F = 0.191/6.59 = 0.029$.

Table 2 Calibration of $F \cdot K$ (CO_2) at 35 °C: medians and 90% intervals

Source	Data used	Method	$F \cdot K$	90% interval
Bos et al. (1999)	2 pure-gas values	Monte Carlo, σ = 3%	0.242	0.134–0.356
Bos et al. (1999)	2 pure-gas values	Monte Carlo, σ = 5%	0.243	0.077–0.452
Esposito et al. (2019)	12 mixed-gas values, 25 °C	Bootstrap	0.153	0.066–0.289
Esposito et al., at 35 °C	as above, × 0.948	Bootstrap	0.145	0.062–0.274
Combined (primary)	Bos σ = 3% + Esposito 35 °C	Inverse variance	0.192	0.123–0.272
Combined (conservative)	Bos σ = 5% + Esposito 35 °C	Inverse variance	0.171	0.093–0.276
David et al. (2011a)	Own H_2/CO_2 data	Reported fit	0.859	–

3.3. Temperature dependence

b was held constant with temperature, following the finding of Scholes et al. (2010) that its fitted variation was minimal. $C'_H(T)$ was scaled with the measured heats of sorption (−14.9 kJ mol^{-1} for CO_2, −3.4 kJ mol^{-1} for N_2), valid over the measured 20–75 °C (Scholes et al. 2010). $k_D(T)$ was scaled with the Lennard-Jones correlation used by Scholes et al. (exponent $m = 6.67$) with well depths ε/κ = 195.2 K (CO_2) and 71.4 K (N_2) (Poling et al. 2001); only the ratio $k_D(T)/k_D(35\ °C)$ enters. Diffusion activation energies, for which no independent Matrimid data exist, were calibrated so that the model reproduces the pure-gas permeation activation energies measured by David et al. (2011b) at 4 bar over 30–100 °C (8.1 kJ mol^{-1} for CO_2, 20.2 kJ mol^{-1} for N_2), giving $E_{a,D}$ = 19.19 and 24.16 kJ mol^{-1}. This is a single-target calibration, and F is assumed temperature-independent; both assumptions are tested in Section 4.7. Results above 75 °C use the sorption correlations outside their measured range and are reported as extrapolations.

4. Results and discussion

4.1. Verification

Beyond the analytical reduction (Section 2.2), the module solver satisfied the mass-balance criterion in all runs, converged at first order with N, and gave results independent of dense-layer thickness (Section 2.6; Online Resource 1, Table S1 and Fig. S1b). With the parameters fitted by David et al. (2011a), the transport model reproduces their pure-CO_2 permeabilities at 2–6 bar within 1.1% and their mixed H_2/CO_2 data with a root-mean-square error of 3.2%. Because those parameters were fitted to the same data, this comparison confirms the implementation but does not validate the parameter set; independent tests are reported in Section 4.2. The comparison uses the 35 °C parameter set against data measured at 30 °C.

4.2. F·K calibration and transfer between laboratories

Fig. 1 compares the calibrated model with both datasets. The calibrated value describes the modest pressure dependence of both the pure-gas Bos data and the mixed-gas Esposito data, whereas $F \cdot K = 0.859$ predicts a much stronger decline than either dataset shows. As a held-out test, the fractional root-mean-square error of $F \cdot K = 0.859$ against the Esposito data, which played no part in its derivation, was 0.071, compared with 0.022 for a flat prediction equal to the data mean. The single-laboratory value therefore has no predictive skill on independent data, in this case 3.2 times worse than a constant.

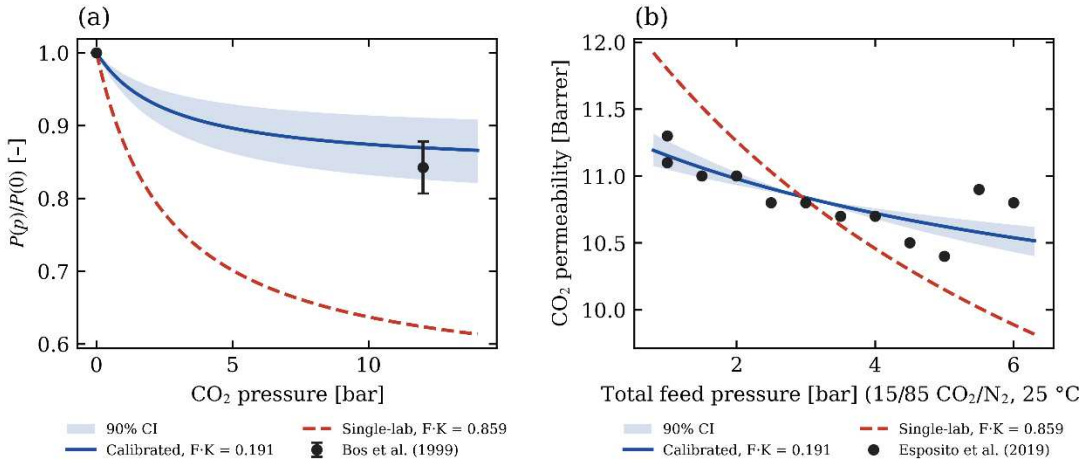


Fig. 1 Calibration of $F{\cdot}K$ against independent data: (a) Pure-CO_2 permeability ratio $P(p)/P(0)$ from Bos et al. (1999) (two reported values; error bar, 3% uncertainty on each permeability). (b) CO_2 permeability in a 15/85 CO_2/N_2 mixture at 25 °C from Esposito et al. (2019). Solid line, calibrated $F{\cdot}K = 0.191$ with 90% band (0.123–0.272); dashed line, single-laboratory value 0.859 (David et al. 2011a)

The distributions in Fig. 2 show that the two independent estimates are compatible: their 90% intervals overlap (0.134–0.356 and 0.062–0.274), and the combined interval, 0.123–0.272, lies wholly below the single-laboratory value, which is outside the plotted range. Applying the same pressure-ratio analysis to the raw pure-gas data tabulated in the companion study of David et al. (2011b) gives $F{\cdot}K \approx 0.69$, while that study's own fitted parameters imply about 1.75. Conversely, the calibrated value does not reproduce the data of David et al. (2011a): with $F{\cdot}K = 0.191$, errors against their pure-CO_2 permeabilities range from −7.7% at 2 bar to +3.3% at 6 bar, and the root-mean-square error against their mixed H_2/CO_2 data is 6.3% (maximum 15.9%), compared with 3.2% for their own fit. No single $F{\cdot}K$ describes the pressure dependence reported by both groups. Estimates derived within one group's data therefore fall in the range 0.69–1.75, and those from two other laboratories fall at or below about 0.36 even at the upper ends of their intervals. The comparison rests on two independent datasets, one of which contributes only two values, so it does not establish a definitive value of $F{\cdot}K$. It does indicate that a dual-mode mobility parameter fitted within one laboratory should not be

assumed to transfer to another, in line with the sensitivity of mixed-gas dual-mode predictions to parameter choice (Ricci and De Angelis 2019; Monsalve-Bravo et al. 2024) and with the inter-laboratory variability of pure-gas permeation data (Mizrahi Rodriguez et al. 2022).

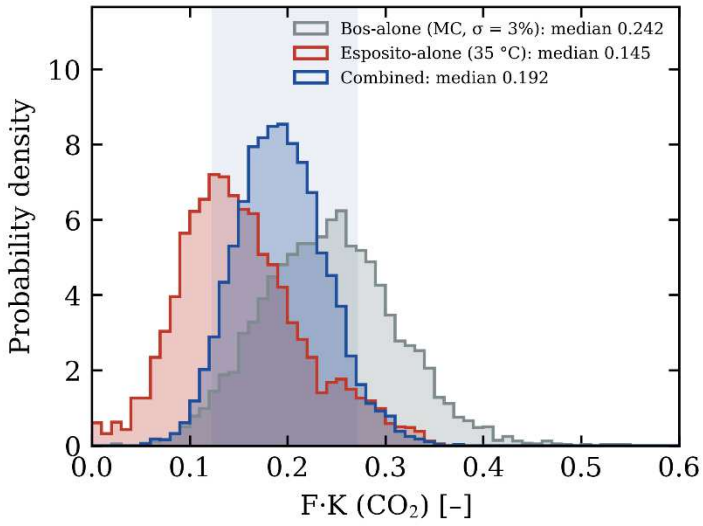


Fig. 2 Distributions of $F{\cdot}K$ (CO_2) at 35 °C: Monte Carlo propagation of the Bos et al. (1999) values (σ = 3%), bootstrap of the Esposito et al. (2019) data converted to 35 °C, and their inverse-variance combination (shaded: combined 90% interval). The single-laboratory value, 0.859 (David et al. 2011a), lies outside the plotted range

4.3. Recovery, purity and area error of a pure-gas design

Table 3 and Fig. 3 report the bias of a design based on pure-gas data at p_{ref} = 1 bar for the baseline flow setting. Across 5–30% CO_2 and 10–20 bar, the pure-gas design overestimated CO_2 recovery by 2.5–3.5 pp, or 1.7–4.8 pp across the $F{\cdot}K$ interval. Relative to the true recoveries of 37–75%, this is an overestimate of about 4–8%. The bias increased with feed pressure but varied little with composition at a given pressure. Purity was overestimated by 0.7–1.2 pp (0.5–1.6 pp across the interval), always with the same sign as and a smaller magnitude than the recovery bias; it was largest at 15% CO_2. With the single-laboratory $F{\cdot}K$ = 0.859 the recovery bias would be 8.6–12.2 pp and the purity bias 2.4–4.1 pp, so the choice of parameter source matters more than the choice of operating condition.

Table 3 True performance and pure-gas design error at a 1 bar measurement pressure

Feed CO_2	p_{feed} (bar)	Rec_B (%)	Pur_B (%)	ΔRec (pp)	ΔPur (pp)	ε_A, 50% / 75% (%)
5%	10	60.73	26.96	2.56 (1.71–3.49)	0.79 (0.53–1.08)	6.1 / 5.6
5%	20	75.19	31.43	3.08 (2.04–4.24)	0.84 (0.56–1.15)	–
15%	10	44.83	65.10	2.53 (1.68–3.48)	1.15 (0.77–1.58)	7.4 / 6.5
15%	20	55.50	70.13	3.46 (2.29–4.76)	1.16 (0.77–1.60)	9.4 / 8.8
30%	10	37.36	86.65	2.56 (1.70–3.52)	0.68 (0.45–0.93)	8.1 / 7.5
30%	20	42.08	88.32	3.40 (2.25–4.70)	0.71 (0.47–0.97)	9.6 / 9.3

35 °C, baseline flow (φ = 5). Bias values at $F{\cdot}K = 0.191$ with the range for $F{\cdot}K = 0.123$–0.272 in parentheses. ε_A, area error at $F{\cdot}K = 0.191$ for target recoveries of 50% and 75%; –, not computed.

The area error places these biases in design terms. To reach 50% or 75% CO_2 recovery, the pure-gas design specified between 5.6% and 9.6% less membrane area than the mixed-gas model required (Fig. 3b). A module built to the pure-gas specification would therefore fall short of its recovery target, or would need a lower feed rate to meet it. At the same target recovery the true permeate was also 1.0–2.1 pp less pure than predicted, which matters where the permeate must meet a compression or transport specification. The area error was larger at 20 bar and at higher CO_2 fractions, and changed little between the two recovery targets.

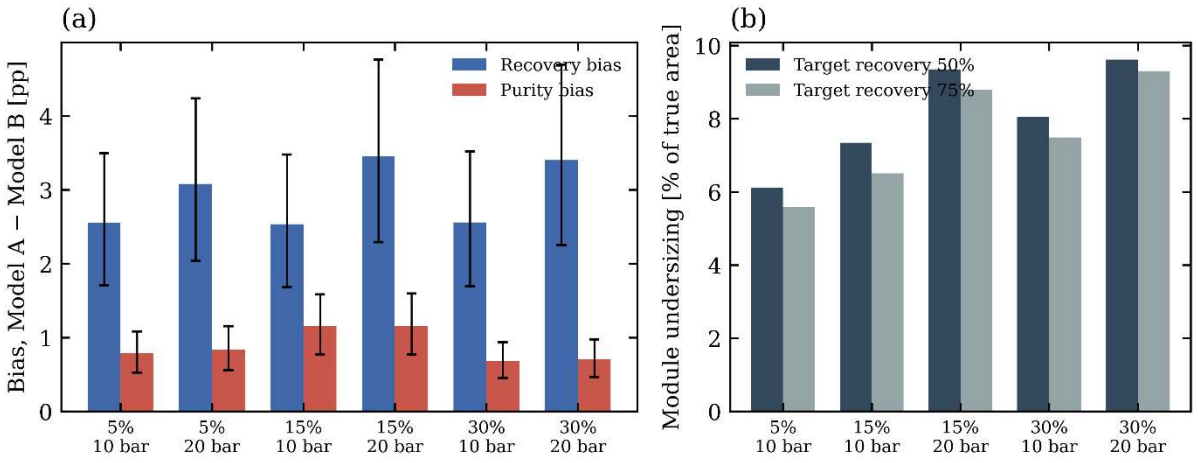


Fig. 3 Recovery, purity and area error of a pure-gas design: (a) Recovery and purity bias of a pure-gas design (p_{ref} = 1 bar) at six feed conditions; error bars span $F{\cdot}K = 0.123$–0.272. (b) Membrane area

omitted by the pure-gas design, as a percentage of the area required by the mixed-gas model, for target CO_2 recoveries of 50% and 75% ($F \cdot K = 0.191$)

The magnitude of the bias depends on operating point. Varying the flow parameter φ from 2 to 10 changed the Model B stage cut from about 21–25% to 6–7% and the recovery bias between 1.0 and 3.5 pp (Online Resource 1, Fig. S1a). The dependence was not monotonic, and at 5% CO_2 and high stage cut the bias fell to 1.0 pp. The values in Table 3 therefore describe the baseline operating point; the sign of the bias was positive in every case examined.

4.4. Correctability boundary

At the baseline operating point and 10 bar feed pressure, the correcting pressure p^* fell steeply as feed CO_2 partial pressure increased (Table 4, Fig. 4). Below about 0.84 bar (90% interval 0.79–0.88 bar) no measurement pressure removed the bias, because even the Henry's-law floor P_∞ gave a higher recovery than the mixed-gas model. Between 0.84 and 1.64 bar a correcting pressure existed but lay between about 750 and 20 bar. Above 1.64 bar (90% interval 1.61–1.66 bar), a pure-gas measurement at or below 20 bar reproduced the true recovery, with p^* approaching about 10 bar at 3–3.5 bar CO_2. In this regime the correcting measurement pressure is 3–12 times the feed CO_2 partial pressure, so a pure-gas test at the feed CO_2 partial pressure would not by itself remove the bias. The practical threshold was insensitive to $F \cdot K$ (±2%), whereas the structural threshold shifted by about ±6%.

Table 4 Correcting measurement pressure p^* at 10 bar feed and baseline stage cut

Feed p_{CO2} (bar)	p^* (bar), $F \cdot K = 0.191$	p^* range, $F \cdot K = 0.123$–0.272	Regime
≈0.05–0.84	n.e.	–	Structural
0.86	748	215 – n.e.	Correctable, impractical
0.90	251	139–928	Correctable, impractical
1.00	94	74–125	Correctable, impractical
1.10	58	50–67	Correctable, impractical
1.30	33	31–35	Correctable, impractical
1.50	23.6	22.7–24.6	Correctable, impractical
1.64	20.0	19.4–20.5	Practical threshold

Feed p_{CO2} (bar)	p^* (bar), $F{\cdot}K = 0.191$	p^* range, $F{\cdot}K = 0.123$–0.272	Regime
2.00	14.9	14.7–15.1	Practical
2.50	12.0	11.9–12.0	Practical
3.00	10.7	10.7–10.8	Practical
3.50	10.3	10.2–10.3	Practical

Stage cut about 10–13% (φ = 5), 35 °C. n.e., no correcting pressure exists (structural regime).

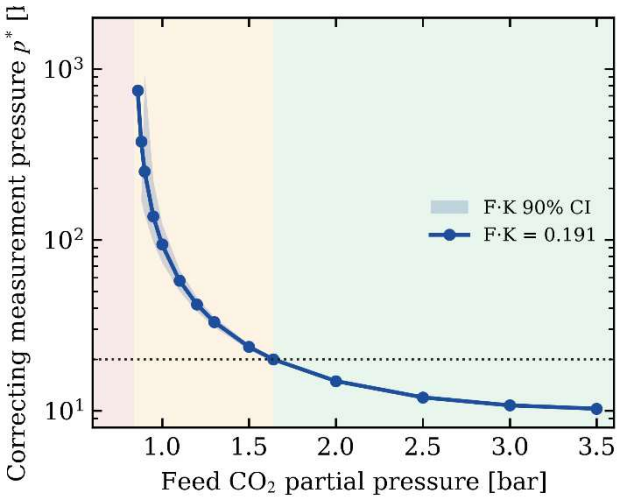


Fig. 4 Correcting measurement pressure p^* versus feed CO_2 partial pressure at 10 bar feed pressure and baseline stage cut (about 10–13%), with the band for $F{\cdot}K = 0.123$–0.272. Shading marks the structural (no p^*), correctable-but-impractical ($p^* > 20$ bar) and practical ($p^* \leq 20$ bar) regimes

These thresholds are not properties of the membrane alone. Fig. 5 maps ΔRec_∞, the recovery bias at the Henry's-law floor, over feed CO_2 partial pressure and Model B stage cut. The structural regime ($\Delta Rec_\infty > 0$) occupied a region bounded above by feed CO_2 partial pressures of about 0.75–0.95 bar across stage cuts of about 4–18%. Its lower edge moved with stage cut: at the baseline it lay near 0.03–0.05 bar, and at a flow setting of φ = 4 (stage cuts of about 13–18%) the structural region spanned only about 0.2–0.7 bar. For φ ≤ 3, corresponding to stage cuts of about 15–44% in the scanned range, no structural region was found, although ΔRec_∞ was small there (−0.01 to −0.27 pp). The practical threshold moved from 1.53 bar at a stage cut of about 4% to 1.84 bar at the highest stage cuts examined. The correctability of a pure-gas design is therefore a joint function of feed composition and operating point, and a threshold

stated in feed CO_2 partial pressure alone applies only to the stage cut at which it was determined.

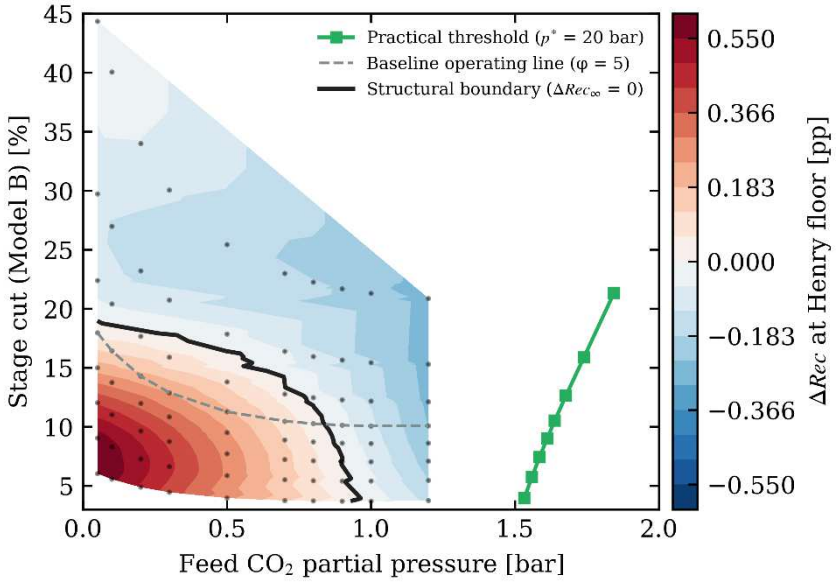


Fig. 5 Correctability regime map at 10 bar feed pressure ($F{\cdot}K$ = 0.191, 35 °C). Colour, recovery bias at the Henry's-law floor, ΔRec_∞ (positive: structural, no correcting pressure). Solid black line, structural boundary (ΔRec_∞ = 0); green squares, practical threshold (p^* = 20 bar); dashed grey line, baseline operating line (φ = 5). Dots mark computed points

The mechanism of the structural regime was examined through the converged axial profiles (Online Resource 1, Fig. S2). In every structural case, the local Model B CO_2 permeability fell below P_∞ = 5.07 Barrer, reaching minima of 4.66–4.85 Barrer at the retentate end, and the Langmuir driving force $C_{H,feed} - C_{H,perm}$ became negative, with minima between −0.12 and −0.29 $cm^3(STP)\ cm^{-3}$. Where this happens, the N_2 partial pressure on the feed face (about 9 bar) suppresses Langmuir sorption of CO_2 much more than the N_2 partial pressure of less than 1 bar on the permeate face, while the CO_2 partial pressure on the permeate face remains a substantial fraction of that on the feed face. The Langmuir population then carries no net CO_2 flux, or a small counter-flux, and the mixed-gas permeability falls below any value a pure-gas

test can return. Falling below the floor locally is necessary but not sufficient for the structural regime: at higher stage cut, 52–58% of the module operated below the floor yet ΔRec_{∞} remained negative, whereas in the structural cases 78–100% of the module did so. The structural regime appears when the below-floor section outweighs the higher-permeability section near the feed inlet.

This mechanism is a direct consequence of applying competitive dual-mode sorption at both membrane faces under local equilibrium. It has not, to the authors' knowledge, been tested experimentally, and the structural regime should be regarded as a model prediction whose confirmation would require mixed-gas permeation measurements at controlled, non-zero downstream CO_2 partial pressure. The practical threshold and the recovery and area biases do not depend on this below-floor behaviour.

4.5. CO_2 self-suppression and N_2 competition

To identify the source of the bias, a third calculation removed N_2 competition ($b_{N2} \rightarrow 0$) while retaining CO_2 self-suppression. The total bias then splits exactly into a CO_2 part, $Rec_A - Rec_{B,noN2}$, and an N_2 part, $Rec_{B,noN2} - Rec_B$, both at $p_{ref} = 1$ bar (Table 5, Fig. 6). At 5% CO_2, the N_2 part (2.79–3.18 pp) exceeded the total, and the CO_2 part was slightly negative (−0.23 to −0.10 pp) because the local CO_2 partial pressure in the module was below the 1 bar measurement pressure. At 30% CO_2, CO_2 self-suppression dominated (1.61–2.61 pp against 0.80–0.94 pp). The two mechanisms therefore exchange dominance with feed composition, and neither can be neglected a priori.

Table 5 Decomposition of the recovery bias into CO_2 and N_2 contributions

Feed CO_2	p_{feed} (bar)	Total	CO_2 part	N_2 part, $F_{N2} = 0$	N_2 part, $F_{N2} = 0.1$	N_2 part, $F_{N2} = 0.2$
5%	10	2.56	−0.23	2.79	5.91	8.12
5%	20	3.08	−0.10	3.18	5.76	7.73
15%	10	2.53	0.64	1.90	3.25	4.19
15%	20	3.46	1.44	2.02	3.00	3.68

Feed CO_2	p_{feed} (bar)	Total	CO_2 part	N_2 part, $F_{N2} = 0$	N_2 part, $F_{N2} = 0.1$	N_2 part, $F_{N2} = 0.2$
30%	10	2.56	1.61	0.94	1.30	1.54
30%	20	3.40	2.61	0.80	1.03	1.18

Values in pp at $p_{ref} = 1$ bar, $F{\cdot}K = 0.191$, 35 °C. The N_2 part is given for the assumed $F_{N2} = 0$ and for $F_{N2} = 0.1$ and 0.2.

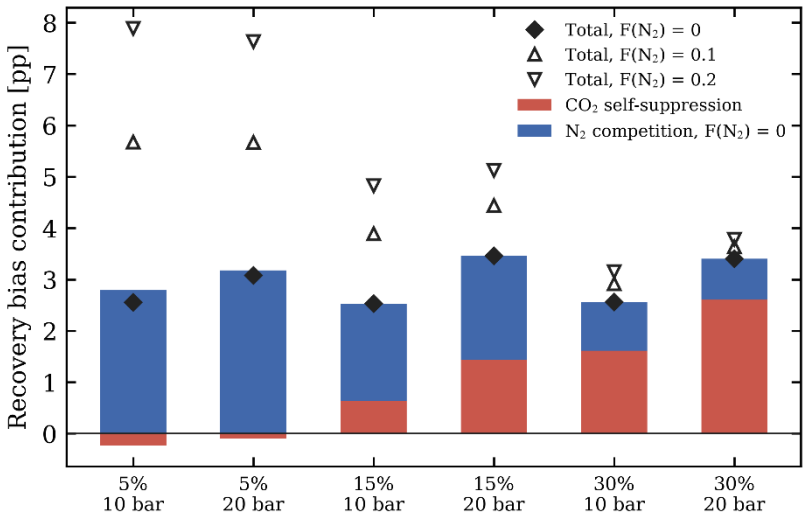


Fig. 6 Decomposition of the recovery bias ($p_{ref} = 1$ bar) into CO_2 self-suppression and N_2 competition for $F_{N2} = 0$ (bars; diamonds, total). Open triangles show the total bias if $F_{N2} = 0.1$ or 0.2

The N_2 part depends strongly on the unmeasured mobility of N_2 in the Langmuir population. With $F_{N2} = 0.1$ or 0.2 it increased to 1.03–5.91 or 1.18–8.12 pp, most strongly for dilute feeds. The dominance of N_2 competition at 5% CO_2 is therefore robust, and the N_2 contributions in Table 5 at $F_{N2} = 0$ are lower bounds.

4.6. Temperature

At 15% CO_2 and 10 bar, the recovery bias fell from 2.56 pp at 30 °C to 2.10 pp at 75 °C, an 18% reduction over the range supported by sorption data, while the ideal CO_2/N_2 selectivity fell 1.9-fold from 32.9 to 17.5 (Fig. 7). Extrapolated to 100 °C, the bias was 1.69 pp (34% below its 30 °C value) and the selectivity 13.2 (2.5-fold lower). Higher temperature reduces the bias because the exothermic Langmuir capacity decreases, reducing the pressure dependence of CO_2 permeation. The selectivity falls faster because the permeation activation

energy of N_2 (20.2 kJ mol^{-1}) is about 2.5 times that of CO_2 (8.1 kJ mol^{-1}) (David et al. 2011b). Raising temperature is therefore not an efficient way to make pure-gas data more reliable.

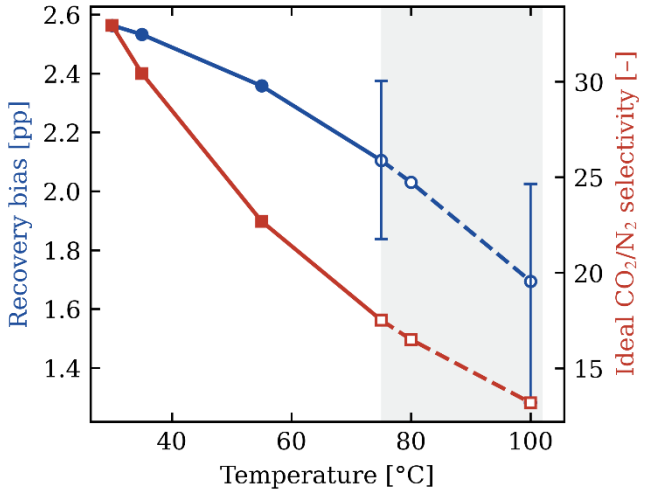


Fig. 7 Recovery bias (p_{ref} = 1 bar) and ideal CO_2/N_2 selectivity versus temperature at 15% CO_2 and 10 bar. Filled symbols and solid lines, 30–75 °C (sorption data range); open symbols and dashed lines, extrapolation. Error bars at 75 and 100 °C span the sensitivity to $F(T)$ and $E_{a,D}$ (Section 4.7)

4.7. Sensitivity to unverified assumptions

Three assumptions lack independent data. First, allowing F to drift linearly by ±20% between 30 and 100 °C changed the reduction in bias over 30–75 °C from 18% to 7–28%, and over 30–100 °C from 34% to 21–47%. Second, perturbing the calibrated diffusion activation energies by ±20% with F constant changed the 30–100 °C reduction to 27–50%. Both sensitivities preserve the direction of the temperature effect, but its magnitude is uncertain by roughly a factor of 1.5 either way. Third, F_{N2} affects the decomposition as described in Section 4.5; because a mobile N_2 Langmuir population adds to the competition effect, the recovery biases reported at F_{N2} = 0 are also likely to be conservative.

4.8. Plasticization

The highest total CO_2 concentration in the conditions studied, at 35% CO_2 and 20 bar, was 23.9 cm^3(STP) cm^{-3} from Eq. (1). This is 51% of the critical plasticization concentration of

Matrimid reported by Bos et al. (47 cm^3(STP) cm^{-3}) (1999) and below the average over the eleven polymers they examined (38 ± 7 cm^3(STP) cm^{-3}). Hollow-fibre studies also indicate that competitive sorption can delay plasticization of Matrimid at moderate pressures (Dong et al. 2011). Plasticization, which the model does not include, is therefore not expected to affect the conditions studied.

4.9. Engineering implications for module design

To make the results usable at the design stage, the regime boundaries of Section 4.4 were mapped onto representative industrial CO_2/N_2 sources (Table 6). Typical CO_2 contents were taken from IPCC (2005), and feed CO_2 partial pressures correspond to compression to the 10 bar feed pressure of the baseline case. The mapping applies to a single counter-current Matrimid stage operated near the baseline stage cut of about 10–13%; at higher stage cut the structural region contracts (Fig. 5), so the classification of dilute feeds is conservative in that direction.

Table 6 Correctability of pure-gas designs for representative CO_2/N_2 sources at 10 bar feed and baseline stage cut

Source (typical CO_2, vol%)	**Feed p_{CO2} at 10 bar (bar)**	**Regime (Table 4, Fig. 5)**	**Implication for design from pure-gas data**
Natural-gas combined cycle (3–4)	0.3–0.4	Structural	No test pressure corrects; mixed-gas data or an explicit area margin required
Coal-fired boiler (12–14)	1.2–1.4	Correctable, impractical (p^* ≈ 28–45 bar)	Correction needs tests above routine range; mixed-gas data preferred
Cement kiln (14–33)	1.4–3.3	Impractical to practical (p^* ≈ 28 down to 10.5 bar)	Above about 16–17% CO_2, a pure-gas test at p^* reproduces true recovery
Second stage of two-stage process, enriched feed (≥ 30)	≥ 3.0	Practical (p^* ≈ 10–11 bar)	Pure-gas data usable if measured near p^*, not at 1 bar

Typical CO_2 contents from IPCC (2005). p^* values interpolated from Table 4 (F·K = 0.191, 35 °C). Boundaries at 10 bar correspond to about 8.4% CO_2 (structural) and 16.4% CO_2 (practical threshold).

The consequence of ignoring the regime can be expressed in equipment terms. For a 15% CO_2 feed at 10 bar, a module sized from 1 bar pure-gas data is predicted to recover 47.4% of the CO_2 but recovers 44.8% (Table 3). Conversely, if a pure-gas design specifies 100,000 m² of

membrane for a 50% or 75% recovery target, the area actually required is 105,900–110,600 m² over the conditions of Table 3, because $A_B = A_A/(1 - \varepsilon_A)$ with ε_A = 5.6–9.6%. At a module cost of the order of US$50 per m² used in capture process studies (Merkel et al. 2010), the omitted membrane alone represents US$0.30–0.53 million per 100,000 m² installed, before the associated pressure vessels, piping and the larger permeate compressor or vacuum pump needed to handle the additional permeate. These figures isolate the dual-mode contribution and are lower bounds where N_2 is mobile in the Langmuir population (Section 4.5).

The results suggest a three-step screening procedure for practitioners. First, compute the feed CO_2 partial pressure and the intended stage cut of each stage. Second, locate the operating point on a regime map of the type in Fig. 5, generated for the polymer and feed pressure of interest with the open code provided (see Data availability). Third, act on the regime: in the practical regime, request or perform the pure-gas test at p^* rather than at the conventional 1–2 bar; in the correctable-but-impractical regime, either perform mixed-gas tests or apply an area margin at least equal to the upper bound of ε_A for that condition; in the structural regime, a pure-gas design cannot be corrected, and mixed-gas permeation data at representative downstream CO_2 partial pressure should be obtained before the module is specified. The procedure requires no information beyond that already used to size the module, and it identifies where limited experimental budgets for mixed-gas testing are most valuable.

Two qualifications apply. Many post-combustion membrane concepts compress the feed only moderately and apply vacuum on the permeate side (Merkel et al. 2010). Such schemes operate at lower feed CO_2 partial pressure and a different pressure ratio from those studied here, and the regime map should be recomputed for them rather than read from Fig. 5. In addition, for multi-stage processes the regime must be assessed stage by stage: in the example of Table 6, a dilute first stage may fall in the structural regime while the enriched second stage of the same process is correctable at routine test pressures.

4.10. Limitations

The results should be read within the following limits. The model neglects pressure drop along the fibre bore and shell and assumes isothermal operation, so Joule–Thomson cooling, which can change permeance appreciably (Ahmad et al. 2013), is excluded; the reported biases isolate the dual-mode contribution and are not a complete account of pure-gas design error. Only $F \cdot K$ was propagated as uncertain; the sorption parameters of Table 1 were fixed. One calibration dataset contributes two values, and the other was measured at 25 °C and converted to 35 °C. The assumption $F_{N2} = 0$ makes N_2 permeability pressure-independent, whereas David et al. (2011b) report a decrease of about 14% between 2 and 6 bar. The structural regime depends on the two-face behaviour discussed in Section 4.4, which awaits experimental confirmation. The analysis covers one polymer and a binary mixture at a single feed pressure for the regime map; other glassy polymers with larger or smaller $F \cdot K$ may shift the boundaries. Finally, the module model has been verified against analytical limits and permeation data but not against measured mixed-gas module performance, which would be the most direct test of the findings. Although no new measurements were made, every comparison in Sections 3.2 and 4.2 is against experimental permeation data from laboratories independent of the source of the sorption parameters, and the held-out test of Section 4.2 is a test against experiment rather than a fit. A direct experimental test of the regime classification would require only a standard constant-pressure mixed-gas permeation cell with a controlled CO_2 partial pressure in a permeate sweep, at two feed compositions on either side of the structural boundary (for example 5% and 25% CO_2 at 10 bar); this is proposed as the decisive experiment.

5. Conclusions

This study examined whether pure-gas permeability data, taken at a suitably chosen pressure, can reproduce the performance of a hollow-fibre module separating CO_2/N_2 with a glassy

polymer that follows competitive dual-mode transport. For Matrimid 5218, a pure-gas design based on 1 bar data overestimated CO_2 recovery by 2.5–3.5 pp and purity by 0.7–1.2 pp at the baseline operating point, equivalent to specifying 5.6–9.6% too little membrane area. The magnitude of this error depends on the mobility parameter $F \cdot K$: a value calibrated against two independent datasets (0.191, 90% interval 0.123–0.272) gave a 1.7–4.8 pp range, whereas a single-laboratory value (0.859) that failed a held-out test would have implied errors three to four times larger.

Whether the error can be removed by the choice of measurement pressure depends on both feed CO_2 partial pressure and stage cut. At stage cuts of about 10–13% and 10 bar feed, no measurement pressure corrects the design below about 0.84 bar CO_2, and a correction within 20 bar requires more than about 1.64 bar. The uncorrectable region contracts as stage cut increases and was not observed above about 18%. It arises because competition on the feed face can drive the local mixed-gas CO_2 permeability below the pure-gas Henry's-law limit, a model prediction that has yet to be tested experimentally. N_2 competition dominates the error for dilute feeds and CO_2 self-suppression for rich feeds, and higher temperature reduces the error at a larger cost in selectivity.

For design practice, the results suggest that pure-gas data can be used for dilute CO_2/N_2 feeds in glassy polymers only with explicit allowance for an area shortfall of the order reported here, that correctability should be assessed at the intended stage cut, and that dual-mode mobility parameters should be calibrated against independent data before being used for design. Priorities for future work are mixed-gas permeation measurements at controlled downstream CO_2 partial pressure to test the below-floor mechanism, an independent determination of N_2 Langmuir mobility in Matrimid, and validation against measured mixed-gas module data. In practical terms, for single-stage operation at 10 bar, pure-gas designs cannot be corrected for natural-gas combined-cycle flue gas, require impractically high test pressures for coal flue gas,

519 and can be corrected by routine testing for enriched feeds and the more concentrated cement-
520 kiln gases. The three-step screening procedure of Section 4.9 allows this classification to be
521 made before a module is sized.

522

523

524

525 **Nomenclature**

Symbol	Definition	Units
a	Membrane area per unit fibre length	$m^2\ m^{-1}$
A, A_A, A_B	Membrane area; area required by Model A, Model B	m^2
b	Langmuir affinity constant	bar^{-1}
C, C_D, C_H	Total, Henry's-law and Langmuir sorbed concentration	$cm^3(STP)\ cm^{-3}$
C'_H	Langmuir capacity	$cm^3(STP)\ cm^{-3}$
D_D, D_H	Diffusion coefficients of Henry's-law and Langmuir populations	$cm^2\ s^{-1}$
$E_{a,D}$	Diffusion activation energy	$kJ\ mol^{-1}$
F	Mobility ratio D_H/D_D	–
F_{in}	Feed molar flow rate	$mol\ s^{-1}$
J	Local molar flux	$mol\ m^{-2}\ s^{-1}$
k_D	Henry's-law coefficient	$cm^3(STP)\ cm^{-3}\ bar^{-1}$
K	Sorption ratio $C'_H b/k_D$	–
l	Dense-layer thickness	m
L	Active fibre length	m
N	Number of axial cells	–
p, p_{ref}, p^*	Pressure; pure-gas measurement pressure; correcting pressure	bar
P, P_∞	Permeability; Henry's-law floor $k_D D_D$	Barrer
Rec, Pur	CO_2 recovery and permeate CO_2 purity	%
y	Feed CO_2 mole fraction	–
z	Axial position	m
ΔRec, ΔPur	Recovery and purity bias, Model A − Model B	pp
ΔRec_∞	Recovery bias with Model A at P_∞	pp
ε_A	Area error, $1 - A_A/A_B$	%
φ	Feed-flow parameter, Eq. (6)	–

526 **Supplementary Information**

Online Resource 1 (ESM_1.pdf): Numerical checks and supplementary figures. Table S1, thickness invariance and grid convergence; Fig. S1, stage-cut sensitivity and grid convergence of the recovery bias; Fig. S2, axial profiles of local permeability and Langmuir driving force.

Abbreviations

CI: confidence interval; MC: Monte Carlo; pp: percentage points; RMSE: root-mean-square error; STP: standard temperature and pressure.

Statements and Declarations

Data availability

The literature data used for model calibration and comparison are available from the cited sources. The code and datasets supporting the conclusions of this article are available in the Zenodo repository, https://zenodo.org/records/23070727

Competing interests

The authors declare that they have no competing interests.

Funding

Not applicable.

Author contributions

MVA: Conceptualization, Methodology, Software, Formal analysis, Investigation, Data curation, Visualization, Writing – original draft, Writing – review & editing, Project administration.

MSO: Methodology, Validation, Investigation, Formal analysis, Writing – review & editing.

GCD: Investigation, Data curation, Visualization, Writing – review & editing.

All authors read and approved the final manuscript.

References

Ahmad F, Lau KK, Shariff AM, Yeong YF (2013) Temperature and pressure dependence of membrane permeance and its effect on process economics of hollow fiber gas separation system. J Membr Sci 430:44–55. https://doi.org/10.1016/j.memsci.2012.11.070

Baker RW, Lokhandwala K (2008) Natural gas processing with membranes: an overview. Ind Eng Chem Res 47:2109–2121. https://doi.org/10.1021/ie071083w

Bos A, Pünt IGM, Wessling M, Strathmann H (1999) CO2-induced plasticization phenomena in glassy polymers. J Membr Sci 155:67–78. https://doi.org/10.1016/S0376-7388(98)00299-3

Bounaceur R, Berger E, Pfister M, Ramirez Santos AA, Favre E (2017) Rigorous variable permeability modelling and process simulation for the design of polymeric membrane gas separation units: MEMSIC simulation tool. J Membr Sci 523:77–91. https://doi.org/10.1016/j.memsci.2016.09.011

David OC, Gorri D, Ortiz I, Urtiaga AM (2011a) Dual-sorption model for H2/CO2 permeation in glassy polymeric Matrimid membrane. Desalin Water Treat 27:31–36. https://doi.org/10.5004/dwt.2011.2041

David OC, Gorri D, Urtiaga A, Ortiz I (2011b) Mixed gas separation study for the hydrogen recovery from H2/CO/N2/CO2 post combustion mixtures using a Matrimid membrane. J Membr Sci 378:359–368. https://doi.org/10.1016/j.memsci.2011.05.029

Dong G, Li H, Chen V (2011) Plasticization mechanisms and effects of thermal annealing of Matrimid hollow fiber membranes for CO2 removal. J Membr Sci 369:206–220. https://doi.org/10.1016/j.memsci.2010.11.064

Esposito E, Mazzei I, Monteleone M, Fuoco A, Carta M, McKeown NB, Malpass-Evans R, Jansen JC (2019) Highly permeable Matrimid®/PIM-EA(H2)-TB blend membrane for gas separation. Polymers 11:46. https://doi.org/10.3390/polym11010046

Heck R, Qahtani, M. S., Yahaya, G. O., Tanis, I., Brown, D., Bahamdan, A. A., Ameen, A. W., Vaidya, M. M., Ballaguet, J.-P. R., Alhajry, R. H., & Mercier, R. (2017) Block copolyimide membranes for pure- and mixed-gas separation. Sep Purif Technol 173:183–192. https://doi.org/10.1016/j.seppur.2016.09.024

IPCC (2005) IPCC special report on carbon dioxide capture and storage. Metz B, Davidson O, de Coninck HC, Loos M, Meyer LA (eds). Cambridge University Press, Cambridge

Khalilpour R, Abbas A, Lai Z, Pinnau I (2013) Analysis of hollow fibre membrane systems for multicomponent gas separation. Chem Eng Res Des 91:332–347. https://doi.org/10.1016/j.cherd.2012.07.009

583 Merkel TC, Lin H, Wei X, Baker R (2010) Power plant post-combustion carbon dioxide capture: an
584 opportunity for membranes. J Membr Sci 359:126–139.
585 https://doi.org/10.1016/j.memsci.2009.10.041

586 Minelli M, Sarti GC (2020) 110th anniversary: gas and vapor sorption in glassy polymeric
587 membranes—critical review of different physical and mathematical models. Ind Eng Chem Res
588 59:341–365. https://doi.org/10.1021/acs.iecr.9b05453

589 Mizrahi Rodriguez K, Wu W-N, Alebrahim T, Cao Y, Freeman BD, Harrigan D, Jhalaria M,
590 Kratochvil A, Kumar S, Lee WH, Lee YM, Lin H, Richardson JM, Song Q, Sundell B, Thür R,
591 Vankelecom I, Wang A, Wang L, Wiscount C, Smith ZP (2022) Multi-lab study on the pure-gas
592 permeation of commercial polysulfone (PSf) membranes: measurement standards and best
593 practices. J Membr Sci 659:120746. https://doi.org/10.1016/j.memsci.2022.120746

594 Monsalve-Bravo GM, G. M., Dutta, R. C., Zuluaga-Bedoya, C. C., Adams, M. P., Smart, S.,
595 Konarova, M., & Bhatia, S. K. (2024) Interpreting gas sorption isotherms in glassy polymers
596 using a Bayesian framework: a view on parameter uncertainty propagation into mixture sorption
597 predictions. J Membr Sci 689:122159. https://doi.org/10.1016/j.memsci.2023.122159

598 Moore TT, Koros WJ (2007) Gas sorption in polymers, molecular sieves, and mixed matrix
599 membranes. J Appl Polym Sci 104:4053–4059. https://doi.org/10.1002/app.25653

600 Paul DR, Koros WJ (1976) Effect of partially immobilizing sorption on permeability and the diffusion
601 time lag. J Polym Sci Polym Phys Ed 14:675–685. https://doi.org/10.1002/pol.1976.180140409

602 Poling BE, Prausnitz JM, O'Connell JP (2001) The properties of gases and liquids, 5th edn. McGraw-
603 Hill, New York

604 Ricci E, De Angelis MG (2019) Modelling mixed-gas sorption in glassy polymers for CO2 removal: a
605 sensitivity analysis of the dual mode sorption model. Membranes 9:8.
606 https://doi.org/10.3390/membranes9010008

607 Scholes CA, Tao WX, Stevens GW, Kentish SE (2010) Sorption of methane, nitrogen, carbon
608 dioxide, and water in Matrimid 5218. J Appl Polym Sci 117:2284–2289.
609 https://doi.org/10.1002/app.32148

610 Thundyil MJ, Koros WJ (1997) Mathematical modeling of gas separation permeators—for radial
611 crossflow, countercurrent, and cocurrent hollow fiber membrane modules. J Membr Sci 125:275–
612 291. https://doi.org/10.1016/S0376-7388(96)00218-9

Supplementary Files

This is a list of supplementary files associated with this preprint. Click to download.

- ESM1.pdf